Experiment Design for Investigation of the Epitaxial Device for Momentum Exchange with the Vacuum State

Contract Report Number 2

Dr. D. C. Hyland
October 15, 2017

Introduction

This study addresses experimental investigation of the author's invention "An Epitaxial device for Momentum Exchange with the Vacuum State" which uses the dynamic Casimir effect to transfer momentum to an object via interaction with the electromagnetic field ground state. Specifically the present work is directed toward preparing the specifications and requirements that would enable a semiconductor, or liquid crystal fabrication firm to build a small-scale test unit of the invention. The effort is divided into four tasks:

1. Thoroughly review and correct, as necessary, the theoretical analysis of the force that can be produced by the device, particularly for the unrestricted (large) amplitude case.

2. Perform design trade-off comparisons, determining force capability, size, dimensions of the laminae, wavelength range, power requirements, etc.

3. Researching the literature to identify semiconductor or liquid crystal devices for which there is a wavelength range where the device can be switched from reflector to transparency, and vice versa. Estimate the achievable active wavelength band, and switching frequency.

4. With a preliminary design, based upon Tasks (2) and (3), formulate the specifications for the manufacturer.

The theoretical review of the fundamental concepts of the epitaxial device was presented at the Advanced Propulsion Workshop held at the Aerospace Corporation, El Segundo, California, November 1-3, 2017, and submitted as the paper "An Epitaxial Device for Dynamic Interaction with the Vacuum State" to the *Journal of the British Interplanetary Society.* This paper constituted the first report under this contract. In this report, we consider the details of the lamina switching algorithm since this topic has considerable impact on the performance specifications developed in this effort. The notations, conventions and basic definitions are those introduced in the first report. We begin with a brief review of the switching formulation and its underlying issues.

Brief Review of the Lamina Switching Concept

It is assumed that within certain wavelength bands, the reflectivity of each lamina can be set within a continuous range from completely reflective to completely transparent. The laminae are also characterized by a finite response time. These features can be combined so that when the laminae are sufficiently closely spaced, and their energizing processes are properly phased, a multi-lamina propagating wave of reflectivity can be created that sustains the properties of a continuously moving mirror.

The finite response time of a semiconductor lamina allows us to create a continuously moving "front" at which the cumulative areal density of charge carriers suffices to produce a desired level of reflectance. Thus, although the laminae are discrete, their sequential stimulus at the proper rate yields the effect of a continuously moving mirror.

Suppose that the conductivity, $\sigma_l(\tau)$, of each individual lamina, in response to a voltage pulse, is uniform through the lamina thickness and has a simple linear rise and fall, as in:

$$\sigma_l(\tau) = \sigma_l^{\max} \begin{cases} \tau/\tau_R, \tau \le \tau_R \\ 2-\tau/\tau_R, 2\tau_R \ge \tau \ge \tau_R \\ 0, \tau > 2\tau_R \end{cases} \tag{1}$$

where τ_R is the finite rise time. $\sigma_l^{\max}$ is the level of conductivity needed to make the lamina perfectly reflective. Suppose each successive lamina is stimulated at a sub-multiple of the rise time after its immediate predecessor, such that each rise in the reflectance is a small fraction of the complete reflectivity. Fig. 1 illustrates the resulting motion of the conductivity profile. An incoming plane wave suffers a cumulative reflection in proportion to the total charge carrier population per unit area along its path. In the example of the figure, the total areal population corresponding to some reflection coefficient, $|R(k)|$, is suggested by the gray-shaded areas. In general, the position of the "front" along which the total reflectance reaches some value is seen to move continuously in the direction of, and with the approximate speed of, the conductivity profile (illustrated by the blue-shaded boundary in the Figure). Even if the charge carrier profile has the staircase form as shown in the Figure, we show below that the effective conductivity profile approximates a continuously increasing distribution. This permits the device to approximate the reflective properties of a mechanical mirror, including the relativistic Doppler effects. Moreover, remaining discretization effects can be mitigated by designing a suitable charge carrier gradient for each lamina.

In the following sections, we determine the conditions on lamina thickness and rise time such that a continuous mechanical mirror can be approximated by a propagating wave.

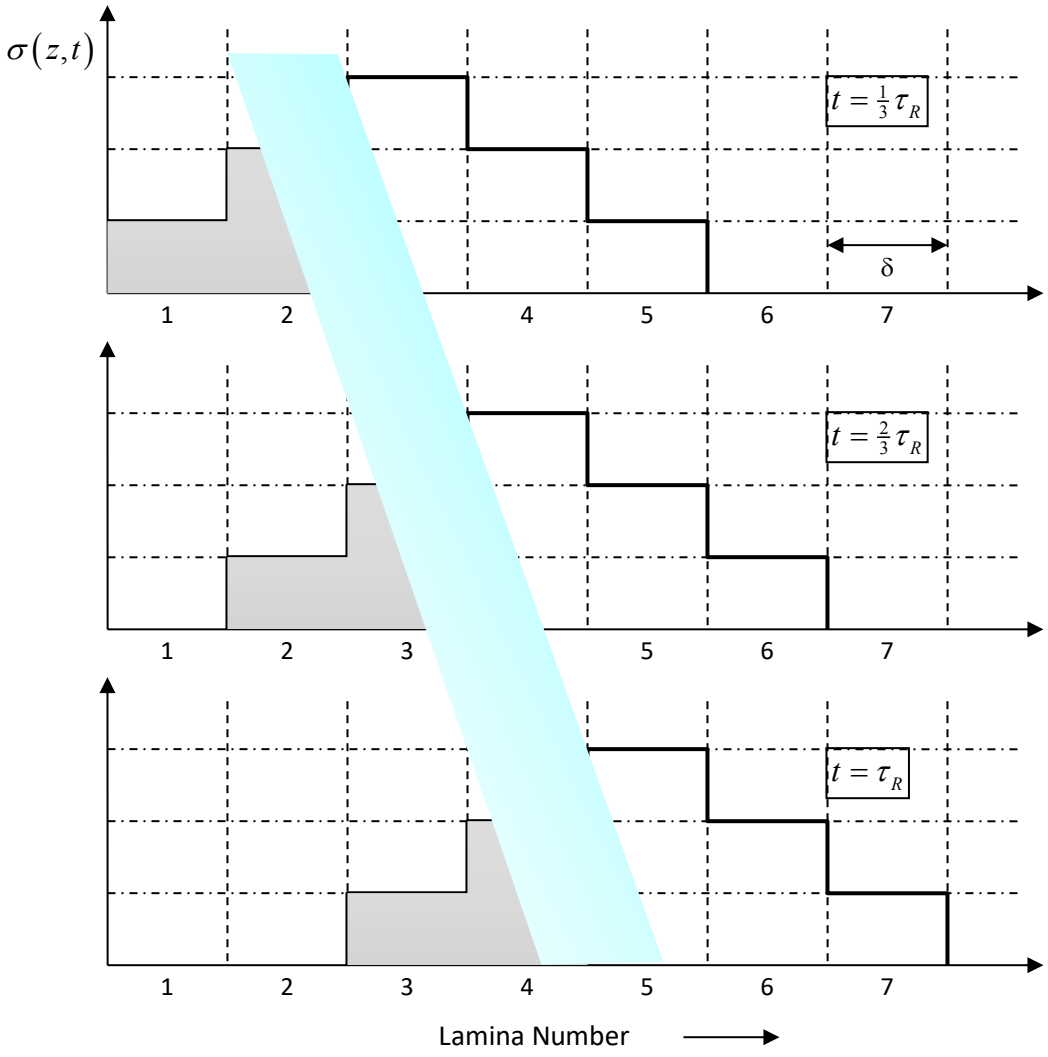

Figure 1. Temporal progression of conductivity as the laminas are successively pulsed. The blue-shaded boundary indicates the continuous motion of the front having a particular value of reflectance.

Basic Formulation of the Reflective Behavior of the Switching Strategy

We consider the behavior of the conductivity profile described above when a vacuum state field mode impinges on the device propagating along the z axis. It suffices to consider the forward portion of the reflectivity wave in Fig. 1, and the incident mode function emanating from the right with wave number *k*. Also one can assume that the electric field is linearly polarized along the x axis; thus:

$$\mathbf{E} = \hat{\mathbf{x}}\Phi(z,\tau), \quad \frac{\partial}{\partial\tau}\mathbf{B} = \hat{\mathbf{y}}\frac{\partial}{\partial z}\Phi(z,\tau) \tag{2.a,b}$$

Then, the general wave equation becomes the well-known telegraph equation:

$$\frac{\partial^2\Phi}{\partial z^2}-\beta\frac{\partial}{\partial\tau}\left(\sigma(z,\tau)\Phi\right)=\frac{\partial^2\Phi}{\partial\tau^2},\quad \beta=\frac{4\pi}{c\varepsilon} \tag{3.a,b}$$

where $\sigma(z,\tau)$ denotes the spatio-temporal distribution across the epitaxial device in accordance with that illustrated in Fig. 1. Because the speed of the front varies slowly during one period, the reflective speed, V, can be assumed constant, and:

$$V=\delta/\tau_S \tag{4}$$

where τ_S is the time required for the conductivity to rise one step. This can be a small fraction of the rise time of the individual laminae.

It is convenient to place the spatial origin at the point $z=V\tau$, and the forward edge of the staircase at the initial time at $z=-\delta$. This is illustrated in Fig. 2. Note that the conductivity distribution looks like a rising escalator. Defining $\xi=z-V\tau$ Equations (2,3) become:

$$\begin{aligned}&\frac{\partial^2\Phi}{\partial\xi^2}-\beta\left(\frac{\partial}{\partial\tau}-V\frac{\partial}{\partial\xi}\right)\left(\sigma(\xi,\tau)\Phi\right)=\left(\frac{\partial}{\partial\tau}-V\frac{\partial}{\partial\xi}\right)^2\Phi\\&E_x=\Phi(\xi,\tau),\quad \left(\frac{\partial}{\partial\tau}-V\frac{\partial}{\partial\xi}\right)B_y=\frac{\partial\Phi}{\partial\xi}\end{aligned} \tag{5.a-c}$$

The boundaries between step changes in the conductivity are located at:

$$\xi=\xi_{b,n}(\tau)=-V\tau\bmod(n\delta),\quad n\in\mathbb{Z}_+ \tag{6}$$

In particular, the forwardmost boundary is at $\xi=\xi_{b,n=1}=\xi_b(\tau)$. At these boundaries, the electric and magnetic fields must be continuous. Also, for $\xi>\xi_b(\tau)$, the incident wave is $\exp\left(-ik\left(\xi+(1+V)\tau\right)\right)$. The approximate boundary condition at $-\infty$ is $\lim_{\xi\to-\infty}\Phi(\xi,\tau)=0$.

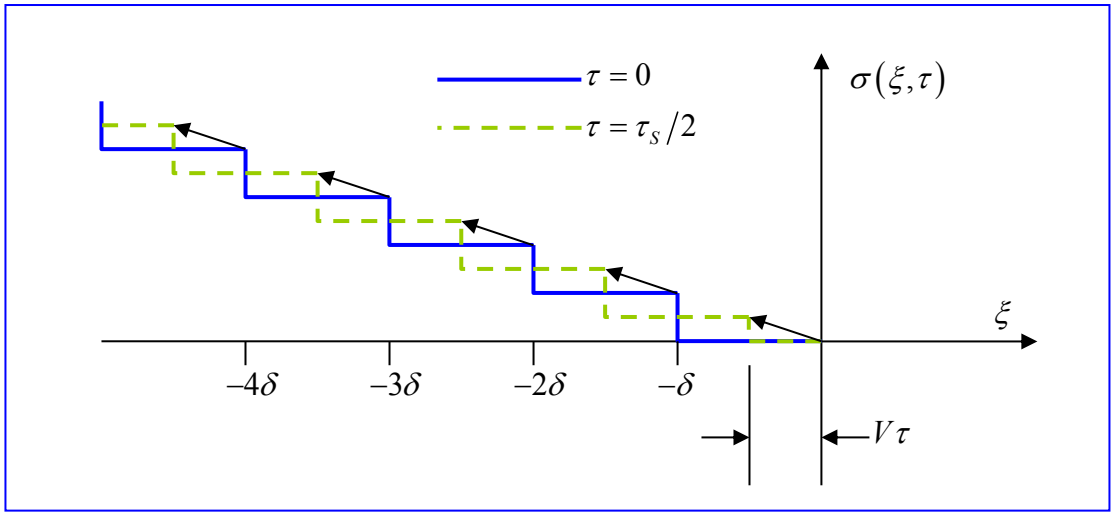

Figure 2. Temporal progression of conductivity as displayed as a function of $\xi=z-V\tau$

Evolution of the Mode Function in the Continuous Limit

First consider the solution to the wave equation when the changes in the conductivity are either continuous or the step changes so small, that $\sigma(\xi,\tau)$ may be approximated by a continuous, linear function. In particular, let γ be a positive, real number, and set:

$$\sigma(\xi,\tau)=\begin{cases}-\gamma\xi, & \xi<0\\ 0, & \xi\geq 0\end{cases} \tag{7}$$

In this case it is obvious that for positive ξ the field must have the form:

$$\Phi(\xi,\tau)=\exp\left[-ik\left(\xi+(1+V)\tau\right)\right]+r\exp\left[-i\hat{k}\left(-\xi+(1-V)\tau\right)\right],\quad \xi>0 \tag{8}$$

where r and $\hat{k}$ denote the reflection coefficient and the wave number of the reflected wave, respectively. For negative ξ the solution to the telegraph equation that vanishes at $\xi\to-\infty$ must be chosen, and this propagates to the left. This gives a time dependence of the form:

$$\Phi(\xi,\tau)=e^{-ia\tau}H(\xi),\quad \xi\leq 0 \tag{9}$$

where a is to be determined.

Using (5.a) and (5.b) and the above formulae, we can determine the continuity conditions at $\xi=0$:

$$\begin{aligned} e^{-ia\tau}H(0)&=\exp\left[-ik(1+V)\tau\right]+r\exp\left[-i\hat{k}(1-V)\tau\right]\\ -\frac{1}{V}\left\{\int_{-\infty}^{0}d\eta\, e^{ia\eta/V}\,\frac{dH(\eta)}{d\eta}\right\}e^{-ia\tau}&=\exp\left[-ik(1+V)\tau\right]-r\exp\left[-i\hat{k}(1-V)\tau\right]\end{aligned} \tag{10.a,b}$$

Consider (10.a). Since the effect of conductivity vanishes at the origin, a must match the wave number of the incident wave in (10.a), i.e. $a=k(1+V)$. Also, since the relation holds for all τ, the second exponent must match the first so that $\hat{k}=k(1+V)/(1-V)$. Note that this is the correct reflection wave number as in the relativistic Doppler effect. Next, making substitutions, we find that $H(0)=1+r$. In summary, (10.a) yields:

$$a=k(1+V),\quad \hat{k}=k\frac{1+V}{1-V},\quad H(0)=1+r \tag{11.a-c}$$

Substituting these results into (10.b), integrating the left-hand side by parts, and defining $h(\xi)=H(\xi)/H(0)$, we have:

$$i(1+V)\left\{\int_{-\infty}^{0} d\eta\, h(\eta)\, \exp\left[ik\frac{1+V}{V}\eta\right]\right\} - V = \frac{1-r}{1+r}V^2 \tag{12}$$

Note that the integral on the left is the Fourier transform of $h(\xi)$. Hence by the Riemann-Lebesque Lemma, the integral approaches zero as $V \to 0$, and (12) is identically satisfied in this limit. We can use (12) to determine r as follows:

$$r = -\frac{(1+V)\Lambda + i(1-V)V}{(1+V)\Lambda + i(1+V)V}$$
$$\Lambda = \int_{-\infty}^{0} d\eta\, h(\eta)\, \exp\left[ik\frac{1+V}{V}\eta\right] \tag{13.a,b}$$

Finally, expressing (5.a) in terms of $h(\xi) = H(\xi)/H(0)$:

$$\frac{d^2}{d\xi^2}h(\xi) - \beta\gamma\left(ik(1+V) + V\frac{d}{d\xi}\right)\xi h(\xi) = \left(ik(1+V) + V\frac{d}{d\xi}\right)^2 h(\xi)$$
$$h(0) = 1, \quad h(\xi) \underset{\xi\to-\infty}{\to} 0, \quad \xi \le 0 \tag{14.a-c}$$

Requiring $\beta\gamma V^2/k << 1$ we perform a perturbation expansion to arrive at the following approximation to the solution to (14):

$$h(\xi) \cong \exp\left[-ik(1+V)\xi - \frac{\beta\gamma V}{8(1+V^2)}\xi^2\right]\left(1 + O\left((\beta\gamma V)^2 V/k\right)\right) \tag{15}$$

This shows that the field magnitude decreases rapidly as the exponential-square with increasing penetration into the epitaxial layers. Using the second expression in (15):

$$\Lambda \cong \sqrt{\frac{\pi(1+V^2)}{2\beta\gamma V}} \tag{16}$$

Thus, if the skin depth of each lamina is relatively large, the factor Λ in (13.a) dominates and there is nearly full reflection $(r \cong -1)$. One the other hand, if Λ is small, since it is real-valued, the magnitude of the reflection coefficient is still of order unity.

From the above development, one can appreciate that a preferred approach would be to have each forward-facing lamina have a negative gradient of $\sigma(\xi)$, and have the back-facing the opposite gradient. If $\sigma(\xi) = \pm V\xi\tau_S/\delta$ then it is obvious from Fig. 2 that the conductivity is continuous and linear across the various laminae, thereby matching the continuous model investigated here. It is not clear that such a design feature is possible, so the next section examines the case in which the conductivity is constant through the thickness of each lamina.

The discussion in this section not only serves to introduce the analysis of the discrete switching scheme of Figs. (1) and (2), it also suggests an alternate, continuous design concept. The linear conductivity profile of Equation (7) can be realized by structuring each lamina to have a linear spatial gradient of conductivity, making the forward end of the pyramidal profile fit condition (7).

Analysis of the Discrete Lamina System

Now consider the reflective properties of the system illustrated in Figs. 1 and 2, in which the conductivity is spatially uniform within each lamina. The conductivity/reflectivity varies step-wise in space, and each step, $\Delta\sigma$, is a small fraction of the value required for total reflectivity. In determining the behavior of the field the most incisive relation, as in the last section, is the continuity of the electric field at the forward boundary. In this case, the forward boundary is $\xi = \xi_b(\tau)$, and on either side of this boundary we have:

$$\begin{aligned} &\xi < \xi_b(\tau): \quad \Phi = f\left(\xi + (1+V)\tau\right) \\ &\xi \geq \xi_b(\tau): \quad \Phi = \exp\left[-ik\left(\xi + (1+V)\tau\right)\right] + g\left(-\xi + (1-V)\tau\right) \end{aligned} \tag{17.a,b}$$

Where $f(...)$ and $g(...)$ are complex-valued, integrable functions. These relations yield the continuity condition:

$$f\left(\xi_b(\tau) + (1+V)\tau\right) = \exp\left[-ik\left(\xi_b(\tau) + (1+V)\tau\right)\right] + g\left(-\xi_b(\tau) + (1-V)\tau\right) \tag{18}$$

Note that since $\Delta\sigma$ and δ are small, $f\left(\xi_b(\tau) + (1+V)\tau\right)$ must be approximately proportional, for all τ, to the incident wave, with some proportionality constant F. Then:

$$g\left(-\xi_b(\tau) + (1-V)\tau\right) \cong (F-1)\exp\left[-ik\left(\xi_b(\tau) + (1+V)\tau\right)\right] \tag{19}$$

Now $g\left(-\xi + (1-V)\tau\right)$ can be expressed in the form:

$$g\left(-\xi + (1-V)\tau\right) \cong R\exp\left[ikS\left(\xi - (1-V)\tau\right)\right] \tag{20.a}$$

Substituting this into (19), we see that since $R\exp\left[ikS\left(\xi_b(\tau) - (1-V)\tau\right)\right]$ must equal $(F-1)\exp\left[-ik\left(\xi_b(\tau) + (1+V)\tau\right)\right]$ for all $\tau > 0$, the function $S\left(\xi - (1-V)\tau\right)$ is determined by:

$$S\left(\xi_b(\tau) - (1-V)\tau\right) = -\left[\xi_b(\tau)(1+V)\tau\right], \bmod(2\pi/k) \tag{20.b}$$

Next, let:

$$\chi = \xi_b(\tau) - (1-V)\tau \quad \Leftrightarrow \tau = \frac{-\chi + \xi_b(\tau)}{1-V} \tag{20.c,d}$$

Using (20.c) in (20.b) produces:

$$S(\chi) = -\frac{2}{1-V}\xi_b\left(\hat{\tau}(\chi)\right) + \frac{1+V}{1-V}\chi, \ \mathrm{mod}(2\pi/k) \tag{21.a}$$

where $\hat{\tau}(\chi)$ is the value of τ, as a function of χ, obtained by repeated substitution of (20.d) into its own right-hand side:

$$\hat{\tau}(\chi) = \frac{1}{1-V}\left(-\chi + \xi_b\left(\frac{1}{1-V}\left(-\chi + \xi_b\left(\frac{1}{1-V}\left(-\chi + \xi_b\left(...\right)\right)\right)\right)\right)...\right) \tag{21.b}$$

(20.a), and (21.a,b) establish the form of the reflected wave. It is apparent that the last term on the right of (21.a) preserves the relativistic Dopper shift of the reflected wave number.

Now consider (21.a). We would like to minimize the quantity $\frac{2}{1+V}\frac{\left|\xi_b\left(\hat{\tau}(\chi)\right)\right|}{|\chi|}$, which is the magnitude of the ratio of the first term to the second. The maximum value of $\left|\xi_b\left(\hat{\tau}(\chi)\right)\right|$ is $V\tau_S$, while the corresponding value of $|\chi|$is δ. To ensure that the reflected wave frequency preserves the Doppler shift, we must require:

$$\frac{2}{1+V}\frac{\left|\xi_b\left(\hat{\tau}(\chi)\right)\right|}{|\chi|} \le \frac{2V}{1+V}\frac{\tau_S}{\delta} < \alpha \tag{22}$$

where α is a positive real number less than unity. In other words, $S(\chi) \cong \frac{1+V}{1-V}\chi$ under the condition:

$$\frac{\tau_S}{\delta} < \alpha\frac{1+V}{2V} \tag{23}$$

This result is not surprising in that the discrete lamina case can be directly formulated as a finite difference approximation to the continuous problem, with τ_S as the time increment and δ as the spatial increment. (23) is the Courant-Friedricks-Lewy condition for the stability of such an algorithm, taking account of the need to adequately approximate the reflected frequency.

Further, one must consider the consequences of the inequality $\left|S(\chi)\right| \le 2\pi/k$, or:

$$\left|-\frac{2}{1-V}\xi_b\left(\hat{\tau}(\chi)\right) + \frac{1+V}{1-V}\chi\right| \le \ 2\pi/k \tag{24}$$

$\xi_b\left(\hat{\tau}(\chi)\right)$is bounded by δ, and setting $\chi = 0$, we find that in order for this inequality to be satisfied, and obtain $S(\chi) \cong \frac{1+V}{1-V}\chi$, we must have:

$$\delta < \alpha \frac{1+V}{2\pi k} \tag{25}$$

Moreover, as α diminishes, the conditions (23) and (25) assure that most finite difference schemes converge to the solution of the continuous case. This implies that these conditions permit the discrete case to well approximate the continuous case.

The corresponding conditions for the analysis of the backward end of the chevron wave in Fig.1 are less restrictive ($\tau_S/\delta < \alpha$) since the reflected wave frequency is smaller than the incident wavenumber. Hence (23) and (25) suffice for this case as well.

To proceed further we determine the details of the extent to which the behavior of the discrete system differs from the continuous case. Referring to Fig.2, the difference between the discrete and continuous distributions is:

$$\begin{aligned}
&\tilde{\sigma}(\xi,\tau) = (\sigma)_{\text{discrete}} - \gamma\xi = \tfrac{1}{2}\gamma\delta\varepsilon(-\xi - V\tau) \\
&\varepsilon(-\xi - V\tau) = \begin{cases} -\dfrac{1}{2\pi}\arg\left(-\exp\left(2\pi i(\xi + V\tau)/\delta\right)\right), & \xi < 0 \\ 0, & \xi \geq 0 \end{cases} \\
&\gamma = V\tau_S\,\xi/\delta
\end{aligned} \tag{26.a-c}$$

$\varepsilon(x)$ may be expressed in the Fourier series:

$$\varepsilon(x) = -\tfrac{1}{\pi}\sum_{n=1}^{\infty}\tfrac{1}{n}\sin(nk_\delta x), \quad k_\delta = 2\pi/\delta \tag{27}$$

Let $\Phi = \Phi_0 + \Phi_1$, where the first term denotes the continuous case field and the second denotes the first term in a perturbation expansion intended to evaluate the effect of $\tilde{\sigma}(\xi,\tau)$. Neglecting second order terms, Φ_1 obeys:

$$\begin{aligned}
\frac{\partial^2\Phi_1}{\partial\xi^2} + \beta\left(\frac{\partial}{\partial\tau} - V\frac{\partial}{\partial\xi}\right)(\gamma\xi\,\Phi_1) - \left(\frac{\partial}{\partial\tau} - V\frac{\partial}{\partial\xi}\right)^2\Phi_1 &= -\frac{\beta\gamma\alpha}{4\pi k}(1+V)\varepsilon(\xi + V\tau)\left(\frac{\partial}{\partial\tau} - V\frac{\partial}{\partial\xi}\right)\Phi_0 \\
&= \frac{(\beta\gamma V)^2\,\alpha}{16\pi k(1+V^2)}(1+V)\varepsilon(\xi + V\tau)\xi\Phi_0
\end{aligned} \tag{28}$$

From this it can be seen that Φ_1 is of higher order in $\beta\gamma V$, and thus imposes no significant additional constraints.

Comparison of the Continuous and Discrete Cases – Graded Lamina Design

The continuous and the discrete switching design concepts have a number of advantages in common. In both cases, the achievable maximum speed of the reflective front can be much greater

than the ratio of the lamina thickness to the switching pulse time. Since the reflective front moves with the chevron pattern of the reflectivity, the relatively gentle grade of the reflectivity means that the actual speed is δ/τ_S divided by the sine of the angle of the conductivity profile. While this requires the use of several lamina to constitute the reflective surface, the benefit is that speeds close to that of light can be achieved with reasonable switching times. Moreover, with appropriate restrictions, both continuous and discrete concepts can duplicate the relativistic Doppler effects of a mechanical mirror.

Regarding the discrete scheme, conditions (23) and (25) impose strong restrictions on the thickness of the lamina and the rise time of the switching process. In contrast, the continuous concept does not need these restrictions since its front-end reflectivity profile is continuous and linear, so that Doppler effects are preserved. Further, it allows thicker lamina and longer switching times to be used to achieve a desired maximum surface speed. An apparent drawback is that, unless the lamina gradient on the backside (down slope of the switching signal) is reversed, the backside conductivity profile is a saw tooth function. However, as is shown in the next section, the lamina gradients can remain the same, without imposing (23) and (25), and without diminishing the propulsive efficiency of the epitaxial array.

The One-Sided Continuous Array – Propulsive Force Analysis

Consider a modification of the conductivity across an individual lamina from spatially uniform, as in Fig. 1, to having a linear increase in the direction opposite to the intended motion of the reflective front. It is assumed that all lamina in the stack are graded in the same way, so that the forward-facing lamina can be arranged to have a continuous, conductivity profile, while the backward facing profile is a saw tooth function, as illustrated in Fig.3.

To achieve a linear profile on the forward side, the energizing pulse time must be coordinated with the conductivity gradient, γ, and the desired front velocity, V. Adopting the previous linear rise/fall model of the energizing pulse given by (1), but including the spatial gradient, and an appropriate time delay for the pulse from lamina to lamina in the forward direction, we have for each lamina:

$$\begin{aligned}
&\sigma_l(z,\tau) = \max\left(0, \sigma_z(z - z_0) + \sigma_\tau(\tau)\right) \\
&\sigma_\tau(\tau) = \sigma_l^{\max}\begin{cases} \tau/\tau_R, \tau \le \tau_R \\ 2 - \tau/\tau_R, 2\tau_R \ge \tau \ge \tau_R \\ 0, \tau > 2\tau_R \end{cases} \\
&\sigma_z\left(z \in (z_0, z_0 + \delta]\right) = -\gamma z, \;\; \gamma = \frac{\sigma_l^{\max}}{N_l\,\delta}
\end{aligned} \tag{29.a-c}$$

where τ_R is the finite rise time. $\sigma_l^{\max}$ is the level of conductivity of each lamina needed to make the front end of the stack as a whole perfectly reflective, z_0 is the left surface of the lamina, and N_l is the number of laminae on the front side of the array (making $2N_l$ partially energized lamina in

total to constitute the reflective front). Allowing our eikonal approximation in which the rate of acceleration during the highest frequency is small, the above distribution, particularly the value given the gradient, γ, will produce a continuous front at the forward half, moving with the speed:

$$V = N_l \delta / \tau_R$$

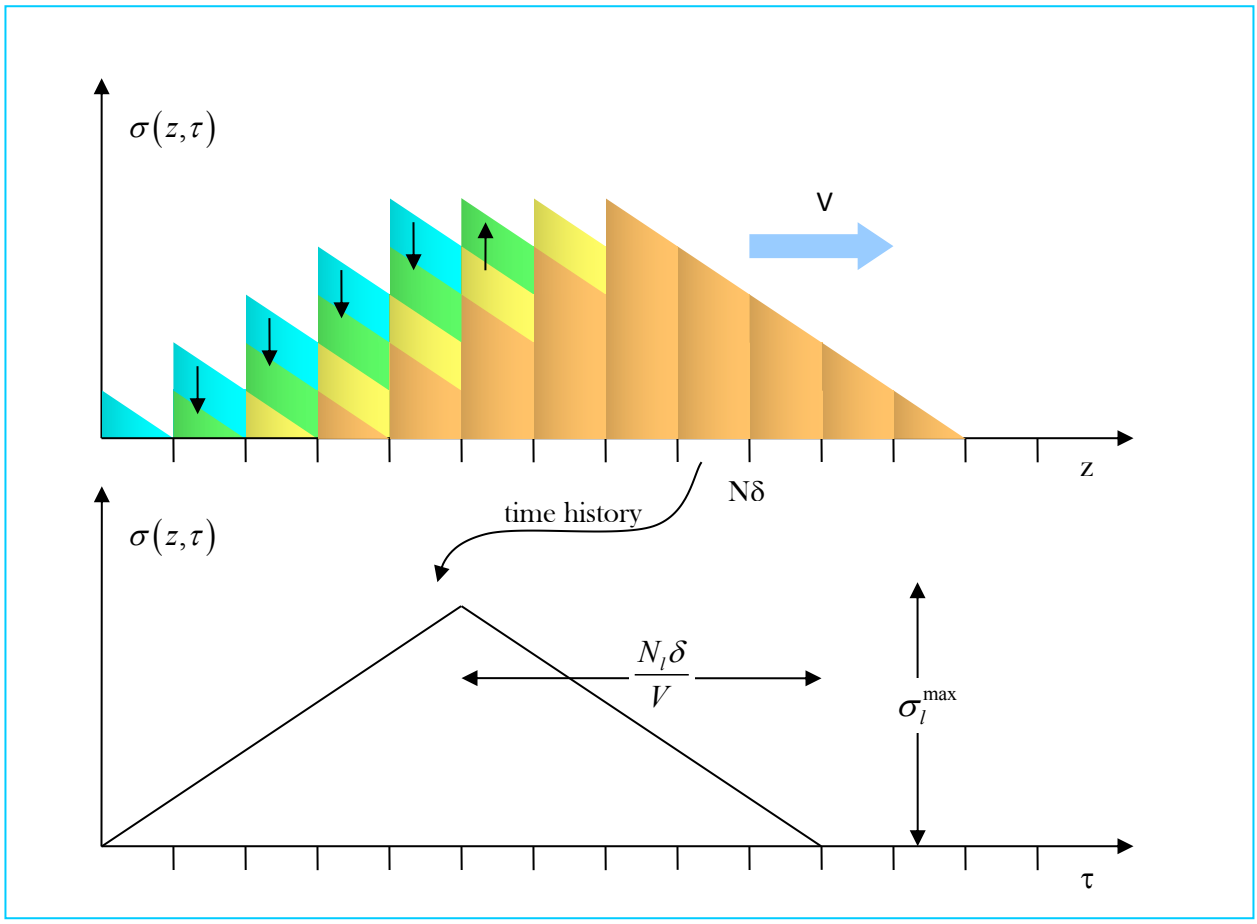

Figure 3. Conductivity distribution and temporal progression for the one-sided continuous array.

Thus, the instantaneous speed is controlled by the pulse duration, $2\tau_R$, which can be adjusted down to the minimum duration, τ_R^{min}, achievable by the electronics. By this strategy, the reflective surface can be made to travel at relativistic speeds using reasonable switching times while reproducing the necessary Doppler shift.

At the same time, however, as Fig. 3 shows, the back end of the energized formation has a saw-tooth configuration that possibly may not satisfy constraints (23) and (25). To determine the impact of this, we assume that the switching time and lamina thickness are much larger than those allowed by (23, 25), then recalculate the propulsive force magnitude first estimated in Report #1.

First, recall the force prediction of the earlier report. The reflective front was idealized by a single, thin surface, with identical properties for both forward and back surfaces. The "active" wavenumber range within lamina could be switched between fully reflective and fully transparent was denoted $k \in (k_L, k_U]$. The recommended scanning motion was a power law acceleration of the form:

$$V(\tau) = \bar{V}(\tau/T)^{N-1}, \bar{V} = N\bar{Z}/T \tag{30.a,b}$$

Where $\bar{Z}$ is the total amplitude of each repetitive scan, T is the duration of each scan period and N is an exponent larger than unity. Note that $\bar{V}$ is the maximum velocity occurring at the end of each scan. It was determined that instantaneous repetition of a scan would produce a temporary "back-wash" that would detract from the total momentum produced. It is better to introduce a pause of $\bar{Z}/c$ before the onset of the next scan. Given these assumptions, the time averaged force is:

$$\begin{gathered}
\langle\langle F_z\rangle/A\rangle_t = \frac{\hbar c}{(4\pi)^2}\bar{\bar{k}}^3\Delta\bar{k}\,\bar{\beta}\,\Lambda(T) \\
\Lambda(T) = \frac{1}{\bar{Z}}\left\{\int_{-T}^{\bar{Z}} d\tilde{\tau}\,\frac{1}{1+V(\tau+\tilde{\tau})} - \int_{\bar{Z}}^{T} d\tilde{\tau}\,\frac{1}{1-V(\tau-\tilde{\tau})}\right\} \\
\bar{\bar{k}} = \left[\tfrac{1}{2}\left(k_U^2 + k_L^2\right)\cdot\tfrac{1}{2}\left(k_U + k_L\right)\right]^{1/3} \\
\Delta\bar{k} = k_U - k_L \\
\bar{\beta} = 2\bar{Z}/(T+\bar{Z}) \in [0,1)
\end{gathered} \tag{31.a-e}$$

The second term in $\Lambda(T)$ is the dominant one (the force is in the negative z direction), and is unaffected by the forward reflectivity profile. The first term arises from the backward facing reflective surface, and actually reduces the net force. Let us assume that (23) and (25) are far from satisfied. Then the backward reflection of the vacuum state mode has no Doppler shift. The normalized momentum density is unity, not $1/1+V(\tau+\tilde{\tau})$. This is offset by a decrease in the region over which the momentum density is propagated. The corrected expression for the quantity is:

$$\Lambda(T) = \frac{1}{\bar{Z}}\left\{\frac{N\bar{Z}}{\bar{V}} - \int_{\bar{Z}}^{T} d\tilde{\tau}\,\frac{1}{1-V(\tau-\tilde{\tau})}\right\} \tag{32}$$

A computed comparison of the force predictions is shown in Fig. 4, with the parameters used listed at the top of the chart. It is seen that the one-sided continuous array gives somewhat higher forces at the lower scan rates, but converges to the previous results when maximum forces are close to lightspeed. In any case, however, significant forces are to be attained when the maximum speed approaches unity. In this regime, the previous, thin surface model provides a close lower bound, so that we will continue to use it for subsequent calculations.

In the scheme shown in Fig. 3, the effective $\bar{Z}$ is the total length of travel of the forward end of the reflectivity distribution. This has a delay when the scan first starts, but the process of turning off the

energizing signal can be reserved for the additional time period (see Report #1) set aside for quiescence to avoid force reversal. Therefore, the value of $\bar{\beta}$ in the above need not be altered, and the time duration, $\tilde{T}$, of the complete scan is given by:

$$\tilde{T} = \left(T + \bar{Z}\right)\Big/ 2c = 2\tau_R / c \tag{33}$$

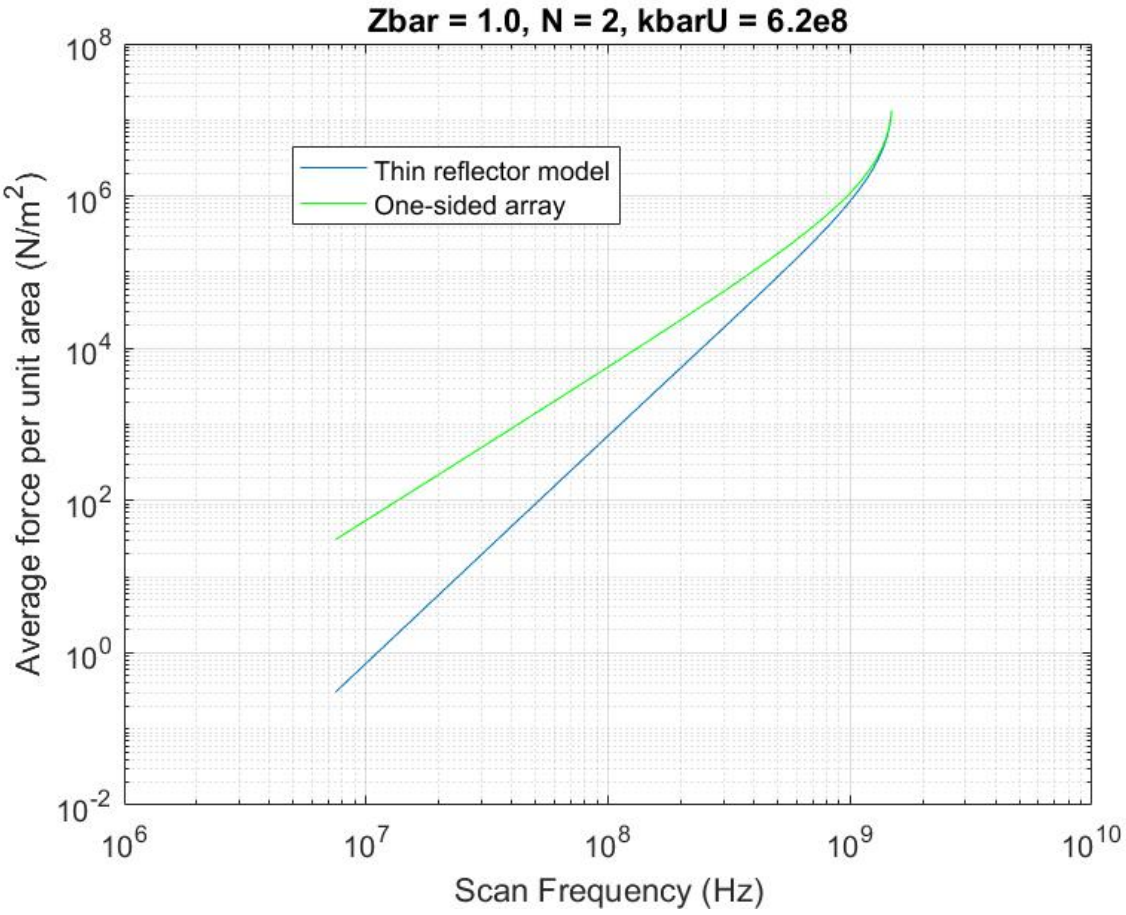

Figure 4. Comparison of forces produced by the idealized thin lamina model and the one-sided continuous array.

Lamina switching can be accomplished by a variety of means, not only by changing the conductivity, as in metallic reflectors. Thus, it is appropriate to specify the necessary lamina maximum reflectivity and relate this to the number of energized lamina, their thickness, and the desired front speed. We first proceed by considering how many lamina there should be in the forward half of the stack to obtain a reflectivity close to one. The quantity in (16) is clearly the *skin depth* of the forward echelon. For $\bar{V}$ close to unity, (13.a) shows that the reflection coefficient is approximately:

$$|r| \cong \frac{\Lambda}{\sqrt{\Lambda^2+1}} = \frac{1}{\sqrt{1+1/\Lambda^2}} \tag{34}$$

To ensure that the reflection coefficient is within about 5% of unity, we require:

$$\Lambda = 3 \;\Rightarrow\; |r| \cong \frac{1}{\sqrt{1+1/\Lambda^2}} = 0.948 \tag{35}$$

From Equation (16) it can be verified that the above reflectivity is a lower bound for all $0 < \bar{V} < 1$.

Now the reflectivity of individual lamina can be accomplished via a variety of processes, not just the modulation of conductivity and charge carrier density in a metal or semiconductor. To preserve all options, it is prudent to specify the acceptable level of total reflectivity of the individual laminae. The treatment of the continuous case makes it clear that the stack reflectivity is the integral of the accumulated reflectivity through the total thickness of the front end. Let r_l be the reflection coefficient of a single lamina. We can approximate the stack reflectivity by:

$$|r| \cong \sum_{k=1}^{N_l} k\, r_l = 1 \Rightarrow r_l \cong \frac{2}{N_l\left(N_l+1\right)} \tag{36}$$

We conclude this section by giving a number of estimates and relationships among the various physical parameters. First, as stated above, the maximum achievable velocity of the reflective surface is related to the lamina thickness, the number of front-end energized lamina, and the minimum possible switching speed, $\tau_R^{\min}$, by:

$$\bar{V} = N_l \delta / \tau_R^{\min} \tag{37}$$

Then we estimate that the minimum required duration of the reflective surface acceleration maneuver is:

$$T \approx 2\,\tau_R^{\min} \tag{38}$$

Then if we select $\bar{V}$ and N we have a specification for $\bar{Z}$:

$$\bar{Z} = T\bar{V}/N \tag{39}$$

Then it follows that the scan frequency is:

$$\Omega_S = \frac{2c}{T+\bar{Z}} = \frac{c}{\bar{Z}}\frac{2\bar{V}}{1+\bar{V}} \tag{40}$$

Design Tradeoffs

The general objective of the study is the determination of specifications for an experimental device consisting of an epitaxial stack of modest dimensions (< 0.3m), capable of producing forces that are

significantly above the threshold of detectability (between 1 and 10 N). To attain these goals the following discussion explains the tradeoffs executed to determine the specific design parameters.

As an initial step, we determine the most efficient surface motion from the class of power law trajectories by examining the behavior of $\Lambda(T)$ for various values of the exponent, N. Fig. 5 shows these results for both integer values above two and fractional values between two and unity.

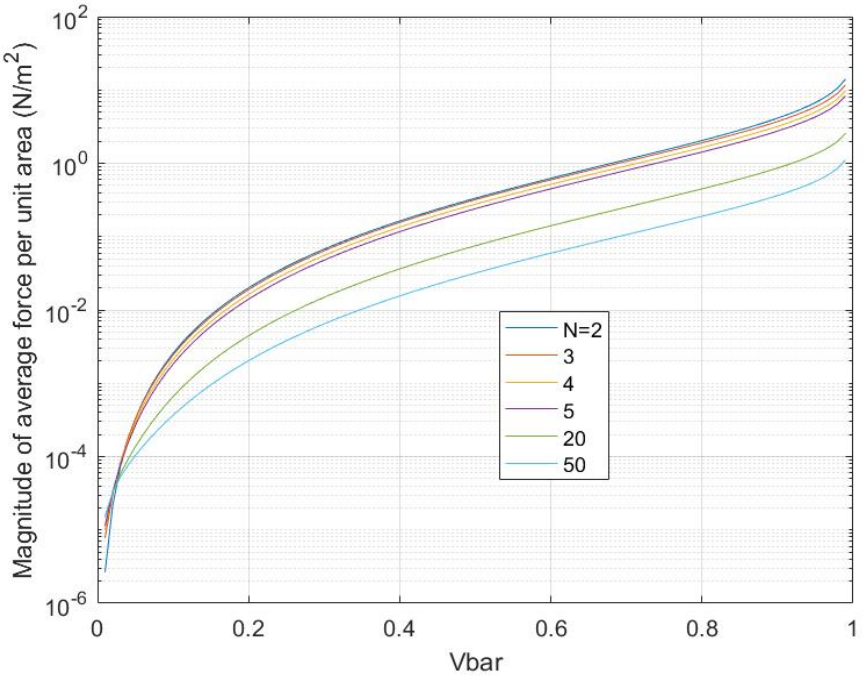

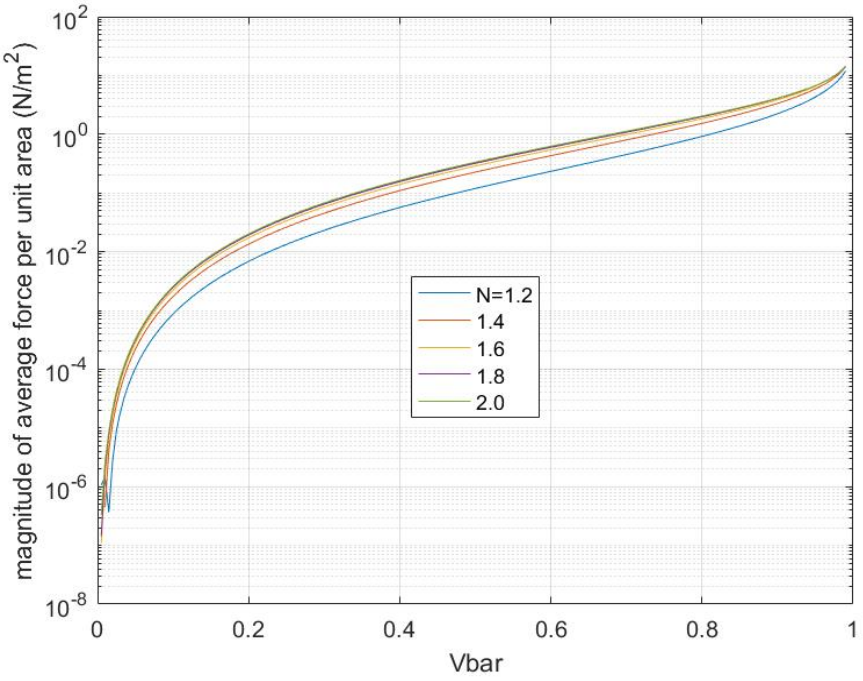

Figure 5. Comparison of forces produced by various exponents in the power law motion profiles

.

It is seen that for all values of $\bar{V}$, $\Lambda(T)$ (and hence the force) attains its maximum value for $N = 2$. Therefore, we adopt this specification.

Perhaps the two most sensitive parameters determining the force magnitude are the maximum speed during the motion trajectory and the upper limit of the wave number range wherein the laminae are switchable (the "active' wavenumber region). The latter is denoted here by k_U. With the $N = 2$ motion profile, we use the estimate of the scan frequency given above. Further, it is assumed that the longest wavelength for which the epitaxial device is active is at the red end of the visual spectrum. The smallest wavelength is chosen to be variable somewhere above the near ultraviolet end of the spectrum (corresponding to a wave number of $2 \times 10^8\ m^{-1}$). The achievable force is especially sensitive to the upper end of the active wave number interval, k_U.

The following plot, Fig. 6, shows the average force per unit area versus scan frequency for $\bar{Z} = 10cm$, and for various values of k_U. The blue line shows what is presently possible with known technology. Clearly, if the active switching wave number could be raised to the extreme ultraviolet, the force would be truly enormous.

It is equally obvious from the chart that to obtain sizable forces, the maximum speed must be a substantial fraction of lightspeed. Since we estimate that silicon-based transistor switching technology is limited to 3 GHz, the force results show that we need a switching speed of about 1 GHz, with $\bar{V} \sim 0.95$, and maximum active regime wave number between near ultraviolet and roughly 30 times that wave number to obtain forces between 1 and 10 N for a device area of $100\,cm^2$. These specifications are adopted forthwith.

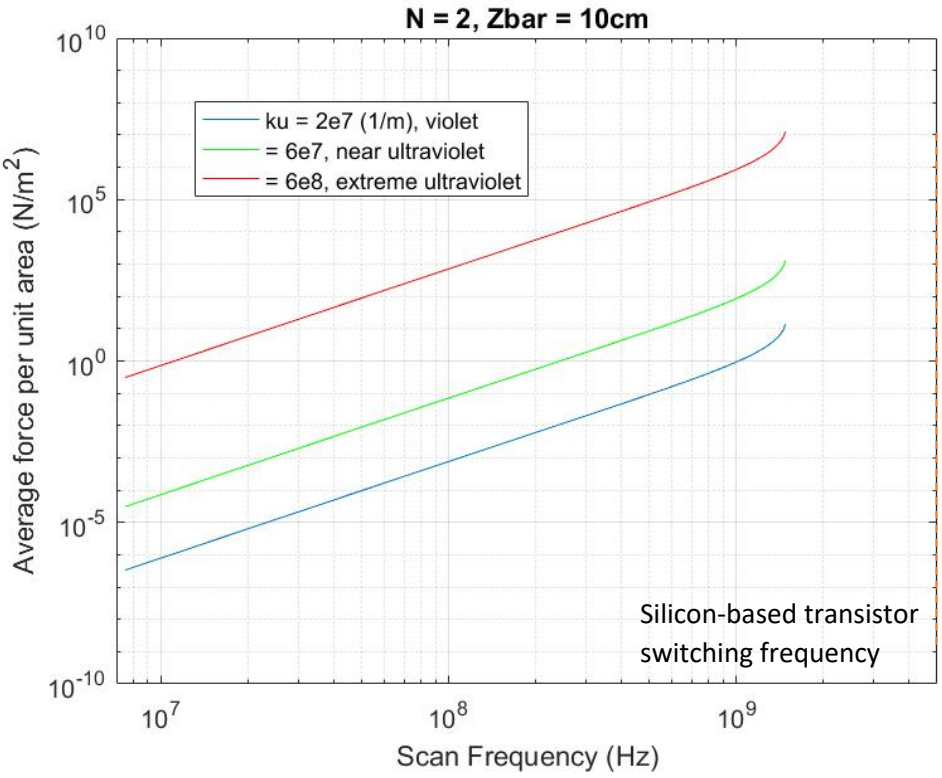

Figure 6. Comparison of forces produced by various values of k_U

It follows from Equation (38) that the duration of the motion wave form is $T = 2\tau_R = 2\,ns$. Further, combining Equations (38) and (40), we have:

$$\bar{Z} = \frac{\Omega_S}{2c} - T \cong 0.06m \tag{41}$$

Similarly, using (37) and (39) to eliminate $\bar{V}$ we obtain:

$$N_l\,\delta \cong \bar{Z} \tag{42}$$

The balance between δ and N_l is a tradeoff of the complexity of producing numerous very thin laminae that have graded reflectivity of sufficient precision, versus a smaller number of thick laminae that may not reproduce the reflective surface acceleration profile with sufficient accuracy. The choice depends very much on the manufacturing processes available. However, to provide a starting estimate, we note that switchable lamina do exist that are as thin as 0.1mm. If we allow for the fact that the lamina reflectivity must be graded to high precision, say to 1%, then we consider a 0.5 mm thickness. Therefore:

$$N_l \cong \frac{\bar{Z}}{\delta} = \frac{6\,cm}{0.5\,mm} \cong 10 \tag{43}$$

Returning to Equation (36), the minimum reflectivity required of each lamina is only:

$$r_l \cong \frac{2}{N_l\left(N_l+1\right)} > 0.02 \tag{44}$$

This rather unrestrictive requirement could have the benefit that more intense design effort could be placed in improving the degree of transparency of the unenergized lamina, rather than the reflectivity. However, imposing a small bound on reflectivity requires considerable precision. Thus, it is prudent to raise estimate (44) to 20%.

Regarding the in-plane dimensions of the epitaxial device, Casimir edge effects need some consideration. Report 1 assumed that the in-plane dimensions were much larger than the stack thickness, so that one-dimensional approximations could be used. However, a one-sided continuous design depends only on the Casimir thrust generated by the forward end of the echelon reflectivity distribution. In this case, when the maximum speed is close to lightspeed, the reverberant mode function has its momentum density vector close to the surface normal. As a crude estimate, edge effects may not be significant as long as the in-plane dimension, denoted by L_l, is at least:

$$L_l \approx \left(1+\sqrt{2}\right)\delta = 14\,cm \tag{45}$$

It is immaterial whether the in-plane shape of the stack is square or circular. For performance predictions we assume the latter case, with L_l serving as the diameter.

Summary of Parameter Estimates

The following table summarizes the nominal values of the design parameters so far estimated

Table 1: Parameter Estimates

Quantity	Definition	Nominal Value
N	Exponent in the power law acceleration profile	2
k_U	Upper end of the active wave number range	$2\times10^8\ m^{-1}$
k_L	Lower end of the active wave number range	$0.3\times10^8\ m^{-1}$
Ω_{max}	Maximum scan frequency	$1\,GHz$

τ_R	Minimum switching pulse rise time	$1\,ns$
$\bar{V}$	Maximum speed in the acceleration profile	$0.95\,c$
$\bar{Z}$	Total force producing stroke of the acceleration profile	$6\,cm$
N_l	Number of lamiae	>10
δ	Lamina thickness	$5\,mm$
r_l	Maximum lamina reflectivity	>0.2
t_l	Unenergized lamina transparency	0.995
L_l	Circular lamina diameter	$14\,cm$

Force Production Estimates and Sensitivities

In this section we use Equations (31) to estimate the force capabilities of a design having the nominal parameter values in Table 1 and to investigate the design sensitivities to the most significant parameters. The blue curve in Fig. 7 shows the force as a function of the scan frequency for the nominal parameter values. It turns out that the nominal scan frequency results in 10N, nearly exactly. It is apparent that there is the flexibility to increase the scan rate by a factor of two,, in which case the force is increased by over an order of magnitude. Roughly the same rate of diminution occurs when the same factor reduces the scan rate. In similar manner, the red and green curves show the effects of reducing and augmenting, respectively, the nominal upper limit of the active wave number range by a factor of two. This rate of variation changes the force by a factor of approximately 20 in either direction. Performance is clearly most sensitive to k_U.

In contrast, Figure 8 shows the corresponding results when the lower limit, k_L, is varied from its nominal value of roughly $1/6$ of k_U. There is the same sensitivity to scan rate, but insignificant variation in the force when k_L is changed by a factor of two.

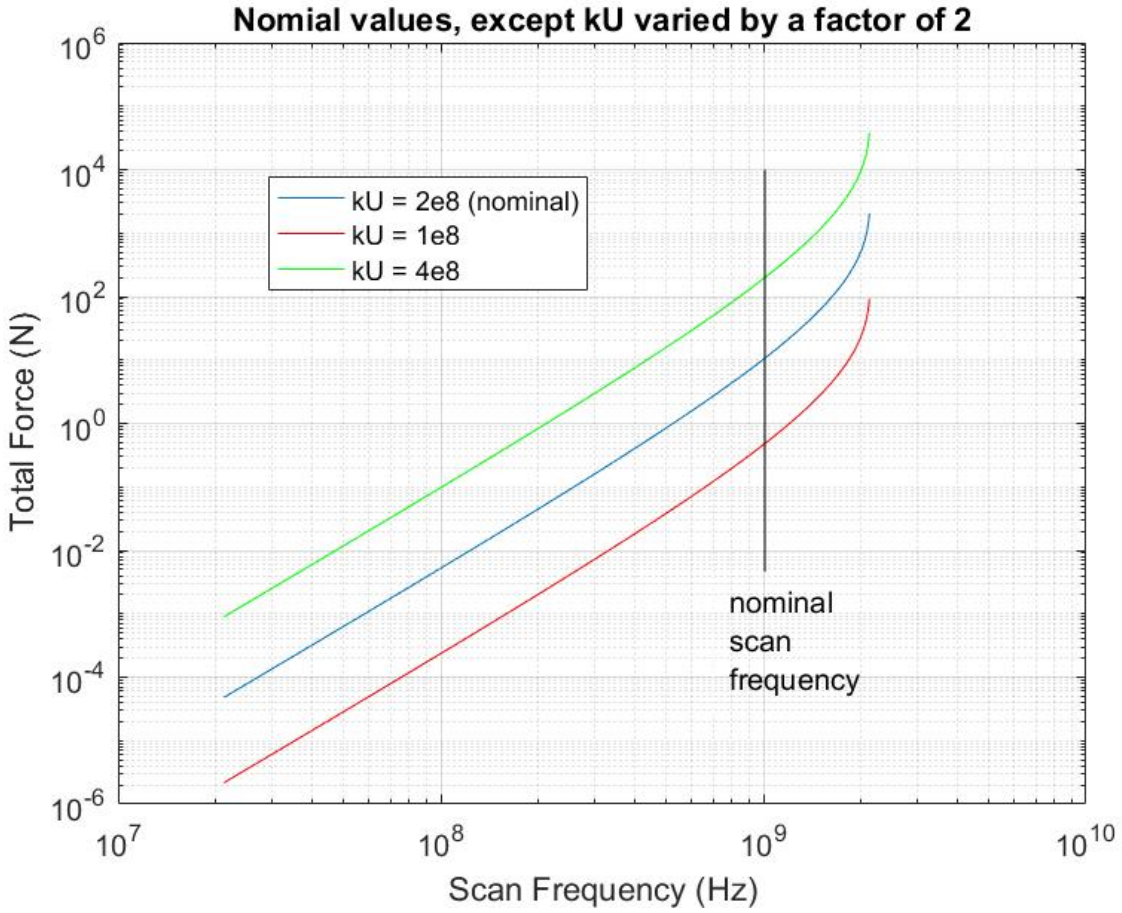

Figure 7. Calculation the force produced by the nominal design, compared with the results produced by varying k_U

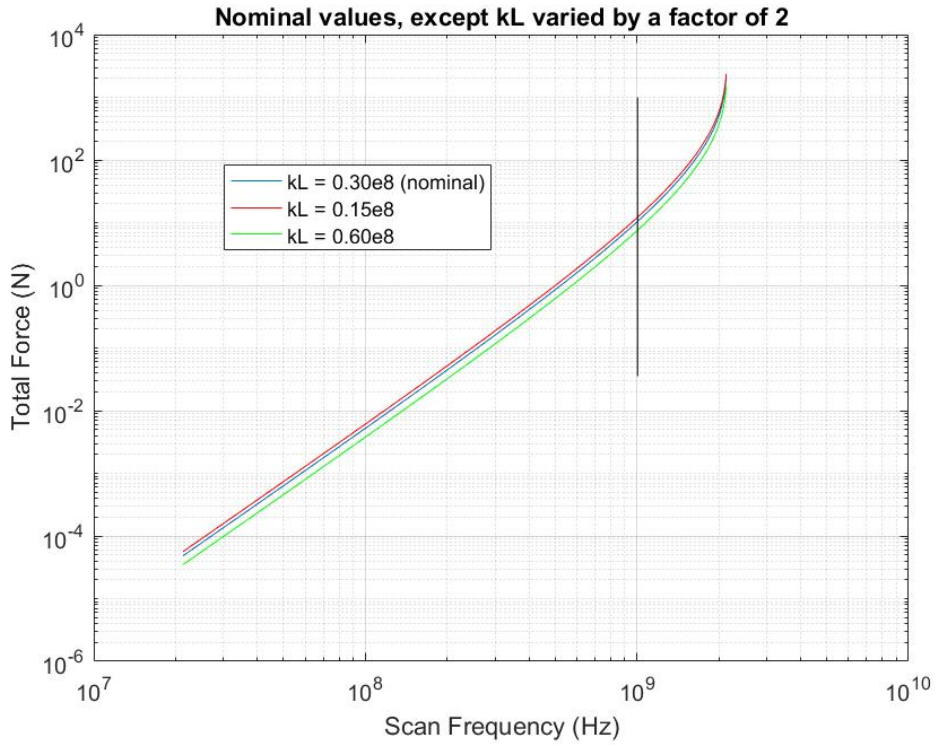

Figure 8. Calculation of the force produced by the nominal design, compared with results produced by varying k_L

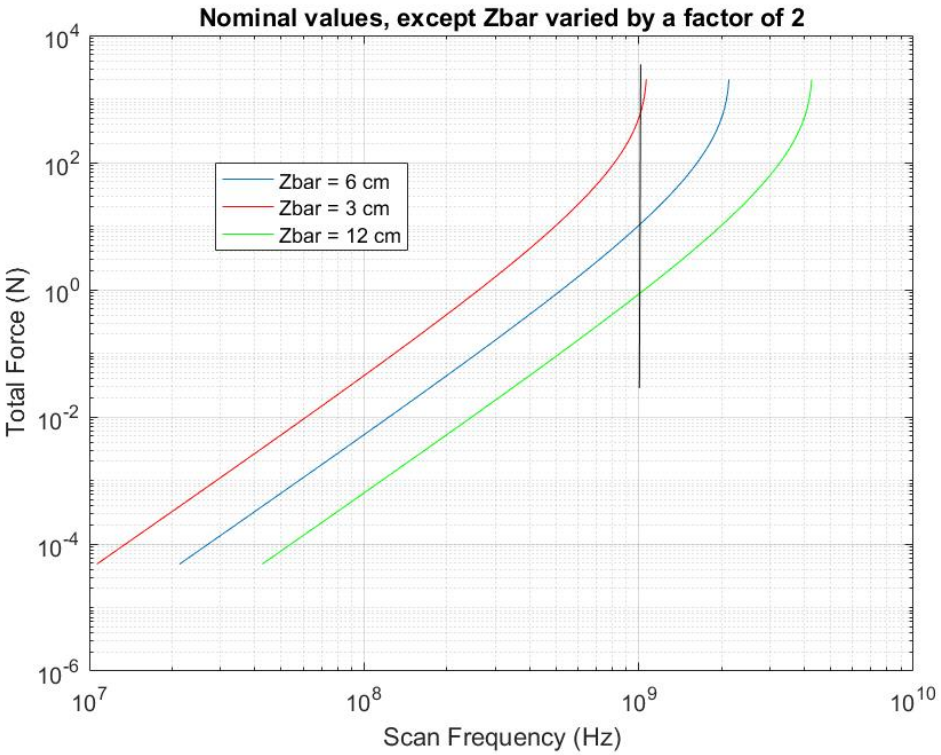

Figure 9. Calculation of the force produced by the nominal design, compared with the results produced by varying $\bar{Z}$

Fig. 9 shows the effect of varying the stroke length of the acceleration profile, $\bar{Z}$. Note that when we keep the scan rate the same but decrease the stroke length, a higher peak velocity is required. Thus, the several curves in Fig. 9 are shifted horizontally, along the scan frequency axis. The lower than nominal $\bar{Z}$ requires a maximum speed quite close to lightspeed, such that at the nominal scan rate, the force curve leaves its power law regime and enters the close-to-lightspeed divergence. Consequently, at the nominal scan frequency, the red curve raises the force by a factor of roughly 50 over the nominal result. In contrast, the green curve in Fig. is only ten-fold below the nominal.

With regard to the other significant parameters listed in Table 1, the force obviously increases as the square of the diameter, L_l. Changes in δ and N_l will not affect performance appreciably as long as they are varied in inverse proportion. The product of lamina reflectivity and the number of laminae must be at lease the nominal. Finally the difference between the unenergized transparency and unity can reduce the force by as much as $\left(1-t_l\right)^{N_l}$. The nominal value of t_l is chosen so that $\left(1-t_l\right)^{N_l}$ is slightly above 90%.

Conclusion

In this report, an in-depth investigation of the lamina switching algorithm was performed. From the performance analysis, details of the switching algorithm were refined, and the greatly improved "one-sided continuous array" design was developed. The updated design significantly reduces the device complexity and fabrication precision required while permitting much higher peak accelerations of the motion profile (hence, higher force outputs). Integrating these refinements with the design, we performed trade-off analyses considering the more than dozen significant design parameters. A nominal design was developed meeting our goal of 1N to 10N force produced by a test device with size scale about 10cm. The sensitivities of this design to variations in the design parameters was explored. Within the state of our present knowledge, the nominal design can attain performance well above the edge of detectability, and there is considerable latitude in selecting design parameters to sustain this capability.